On the Accuracy of First-Order Numerical Derivatives in Multidimensional Digital Waveguide Mesh Topologies

Hüseyin Hacıhabiboğlu, *Member, IEEE*, Banu Günel, *Member, IEEE*, and Ahmet M. Kondoz, *Member, IEEE*

***Abstract*—Digital waveguide mesh (DWM) models are numerical solvers for the wave equation in N-dimensions. They are used for obtaining the traveling-wave solution in practical acoustical modeling applications. Although unstructured meshes can be used with DWMs, regular mesh topologies are traditionally used due to their implementation simplicity. This letter discusses the accuracy of first-order approximations to numerical derivatives on more general unstructured mesh topologies. The results are applied to structured, regular mesh topologies as used in DWM modeling. A comparison of 2-D and 3-D DWM topologies with respect to the accuracy of first-order approximations to numerical derivatives is presented.**

***Index Terms*—Acoustic signal processing, acoustical modeling, digital waveguides, finite difference methods, multidimensional sampling, numerical derivatives.**

I. Introduction

As a numerical solver for the wave equation, the digital waveguide mesh (DWM) approach is used in a variety of audio synthesis and acoustical modeling contexts including the vocal tract [1], musical instruments [2], [3], and room acoustics [4], [5]. DWM approach is equivalent to transmission line modeling (TLM) and finite-difference time-domain (FDTD) methods [6]. Although it is sufficient to use a 1-D DWM for simpler modeling problems such as string instruments and the vocal tract, multidimensional DWMs are used in other modeling problems such as the modeling of a drum membrane or the acoustics of a room due to their inherent multidimensionality.

It is possible to obtain the pressure, p, and velocity, $\mathbf{v}$, components of a modeled acoustical field on discrete junctions on a DWM. While these components are sufficient to define the acoustical field at a given position in space, other acoustical parameters may also be calculated from DWMs with reference to the linear acoustic equations and the acoustic-energy corollary. In particular, the following parameters may be derived among others:

$$\text{Rate of change of fluid density}: \quad \frac{\partial \rho}{\partial t} = -\rho_0 \nabla \cdot \mathbf{v}$$

$$\text{Rate of change of velocity}: \quad \frac{\partial \mathbf{v}}{\partial t} = -\rho_0^{-1} \nabla p$$

$$\text{Vorticity}: \quad \mathbf{\Omega} = \nabla \times \mathbf{v}$$

$$\text{Rate of change of energy density}: \quad \frac{\partial w}{\partial t} = -p \nabla \cdot \mathbf{v}$$

where ρ is the fluid density after excitation, ρ_0 is the ambient fluid density, Ω is the vorticity, and w is the acoustic energy density [7].

The calculation of all of these acoustical quantities requires the use of the vector operators, gradient (∇), divergence $(\nabla\cdot)$, and curl $(\nabla\times)$, which in turn require partial derivatives of the respective acoustical field component. While the directional derivatives are easy to obtain using a second-order (i.e., three-point) finite difference approximation on rectilinear and cubic mesh topologies due to the intuitive positioning of their junctions, other mesh topologies lack efficient means of calculation for second-order approximations.

This letter presents a comparison of different DWM topologies with respect to the accuracy of first-order approximations to directional derivatives and is organized as follows: Section II presents a method for calculating the directional derivatives on a general unstructured N-dimensional mesh. The approximation errors are also discussed. Section III presents the application of the results and a comparison of different mesh topologies with respect to the accuracy of numerical derivatives. Section IV concludes this letter.

II. Numerical Derivatives on an Unstructured Mesh Grid

Although the use of unstructured mesh topologies with finite difference methods is not a new concept [8], they are traditionally not used with DWM models due to the difficulties in using fractional delays for each bidirectional delay element in the mesh. However, the calculation of the numerical derivatives is given for unstructured meshes in this section without loss of generality.

A. First-Order Finite Difference Approximation

Let us have a sample point $\mathbf{x_0} \in \mathbb{R}^N$ with M neighboring sample points $\{\mathbf{x_i} \in \mathbb{R}^N : i = 1 \cdots M\}$ on an N-dimensional

Manuscript received August 17, 2007; revised September 25, 2007. The work presented was developed within VISNET II, a European Network of Excellence, funded under the European Commission IST FP6 programme. The associate editor coordinating the review of this manuscript and approving it for publication was Prof. Vesa Välimäki.

The authors are with Multimedia and DSP Research Group (I-Lab), Centre for Communication Systems Research (CCSR), University of Surrey, Guildford GU2 7XH, U.K. (e-mail: h.hacihabiboglu@surrey.ac.uk; b.gunel@surrey.ac.uk; a.kondoz@surrey.ac.uk).

Digital Object Identifier 10.1109/LSP.2007.911162

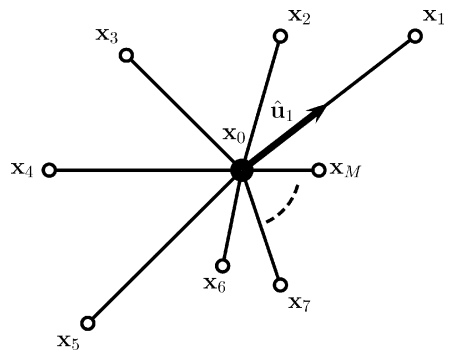

Fig. 1. Node and M neighboring points in an arbitrary N-dimensional unstructured grid. $\hat{\mathbf{u}}_i$ denotes the unit vector in the direction of the ith neighbor.

unstructured mesh grid. Let us also define the N-dimensional displacement vectors, $\overline{\mathbf{r}_i}$, such that

$$\overline{\mathbf{r}_i} = \mathbf{x}_i - \mathbf{x}_0 = \|\overline{\mathbf{r}_i}\|\hat{\mathbf{u}}_i \tag{1}$$

where $\hat{\mathbf{u}}_i = [u_{i,0}\ u_{i,1}\ \cdots\ u_{i,N-1}]$ for $i = 1 \cdots M$ is the unit vector in the direction of the neighboring sample point in N-dimensional hyperspherical coordinates, and $\|\bullet\|$ denotes the Euclidean norm of the vector. The unit vector $\hat{\mathbf{u}}_i$ in hyperspherical coordinates can be represented in the Euclidean space as

$$\begin{aligned}
u_{i,0} &= \sin\phi_{i,1}\sin\phi_{i,2}\cdots\sin\phi_{i,N-2}\sin\phi_{i,N-1}\\
u_{i,1} &= \sin\phi_{i,1}\sin\phi_{i,2}\cdots\sin\phi_{i,N-2}\cos\phi_{i,N-1}\\
&\vdots\\
u_{i,N-2} &= \sin\phi_{i,1}\cos\phi_{i,2}\\
u_{i,N-1} &= \cos\phi_{i,1}
\end{aligned} \tag{2}$$

where $\{\phi_{i,k}\}$ represents the angular coordinates of the hyperspherical coordinate system. Fig. 1 shows the unstructured mesh grid topology.

For an N-dimensional, real, differentiable function $f(\mathbf{x})$ sampled on the described grid, a two-point first-order approximation to the directive derivatives can be formed for each neighboring point, $\mathbf{x}_i$, of the central point, $\mathbf{x}_0$, such that

$$D_{\hat{\mathbf{u}}_i} f(\mathbf{x}_0) = \frac{f(\mathbf{x}_i) - f(\mathbf{x}_0)}{\|\overline{\mathbf{r}_i}\|}. \tag{3}$$

This approximates the gradient of the function, $f(\mathbf{x})$, in the direction of $\hat{\mathbf{u}}_i$. Therefore, the first-order finite difference approximation is a predictor of the following projection of the gradient in that direction:

$$\nabla f(\mathbf{x})|_{\mathbf{x}=\mathbf{x}_0} \cdot \hat{\mathbf{u}}_i \simeq D_{\hat{\mathbf{u}}_i} f(\mathbf{x}_0). \tag{4}$$

It is then possible to express the ensemble of these approximations as a set of linear equations such that

$$\mathbf{D}f(\mathbf{x}_0) \simeq \mathbf{U}\mathbf{d}f(\mathbf{x}_0) \tag{5}$$

where

$$\mathbf{D}f(\mathbf{x}_0) = [D_{\hat{\mathbf{u}}_1} f(\mathbf{x}_0) D_{\hat{\mathbf{u}}_2} f(\mathbf{x}_0) \cdots D_{\hat{\mathbf{u}}_M} f(\mathbf{x}_0)]^{\mathbf{T}} \tag{6}$$

$$\mathbf{U} = \begin{bmatrix} u_{1,0} & u_{1,1} & \cdots & u_{1,N-1} \\ u_{2,0} & u_{2,1} & \cdots & u_{2,N-1} \\ \vdots & \vdots & \ddots & \vdots \\ u_{M,0} & u_{M,1} & \cdots & u_{M,N-1} \end{bmatrix} \tag{7}$$

$$\mathbf{d}f(\mathbf{x}_0) = \begin{bmatrix} \dfrac{\partial f}{\partial x_0} & \dfrac{\partial f}{\partial x_1} & \cdots & \dfrac{\partial f}{\partial x_{N-1}} \end{bmatrix}^{\mathbf{T}} \tag{8}$$

and x_i represent the Cartesian coordinates.

For $M < N$, the linear system of equations is underdetermined and a unique solution does not exist, while for $M = N$, a unique solution exists if the matrix $\mathbf{U}$ is not singular (i.e., the equations are linearly independent). For $M > N$, which is also the case for regular mesh grids in two and three dimensions [9], the solution for $\mathbf{d}f(\mathbf{x}_0)$ can be obtained in the optimal sense as

$$\mathbf{d}f(\mathbf{x}_0) = \mathbf{U}^{+}\mathbf{D}f(\mathbf{x}_0) \tag{9}$$

where $\mathbf{U}^{+}$ is the Moore–Penrose pseudoinverse of the matrix $\mathbf{U}$ which is unique for each different positioning of sample points.

B. Approximation Errors

The approximation error, $\epsilon_{\hat{\mathbf{u}}_i}$, for the directional derivative, $D_{\hat{\mathbf{u}}_i}$, is defined as

$$\epsilon_{\hat{\mathbf{u}}_i}(\mathbf{x}) = \nabla f(\mathbf{x}) \cdot \hat{\mathbf{u}}_i - D_{\hat{\mathbf{u}}_i} f(\mathbf{x}). \tag{10}$$

A frequency-domain expression for the error can be obtained by the N-dimensional spatial Fourier transform such that

$$\nabla f(\mathbf{x}) \cdot \hat{\mathbf{u}}_i \xrightarrow{\mathcal{F}_{ND}} \left(\frac{j\overline{\omega} \cdot \overline{\mathbf{r}_i}}{\|\overline{\mathbf{r}_i}\|}\right) F(\overline{\omega}) \tag{11}$$

$$D_{\hat{\mathbf{u}}_i} f(\mathbf{x}) \xrightarrow{\mathcal{F}_{ND}} \left(\frac{e^{-j\overline{\omega}\cdot\overline{\mathbf{r}_i}} - 1}{\|\overline{\mathbf{r}_i}\|}\right) F(\overline{\omega}) \tag{12}$$

where $\overline{\omega} = [\omega_0\ \omega_1\ \cdots\ \omega_{N-1}]$ is the spatial frequency vector with $-\pi < \omega_i \leq \pi$. It is then possible to express the approximation error in the spatial frequency domain as

$$E_{\hat{\mathbf{u}}_i}(\overline{\omega}) = F(\overline{\omega})\mathcal{H}_{\hat{\mathbf{u}}_i}(\overline{\omega}) \tag{13}$$

$$= F(\overline{\omega})\left[\frac{1}{\|\overline{\mathbf{r}_i}\|}(j\overline{\omega} \cdot \overline{\mathbf{r}_i} - e^{-j\overline{\omega}\cdot\overline{\mathbf{r}_i}} + 1)\right]. \tag{14}$$

When the spatial frequency vector is orthogonal to the displacement vector (i.e., $\overline{\omega} \cdot \overline{\mathbf{r}_i} = 0$) or when $\|\overline{\omega}\| = 0$, the corresponding error is zero.

The projection of the approximation errors to Cartesian coordinates can be obtained as in (9) such as

$$\mathbf{E}_x(\overline{\omega}) = \mathbf{U}^{+}\mathbf{E}_u(\overline{\omega}). \tag{15}$$

From (14), it is possible to rewrite (15) such that

$$\mathbf{E}_x(\overline{\omega}) = F(\overline{\omega})\mathbf{U}^{+}\mathbf{H}_u(\overline{\omega}) \tag{16}$$

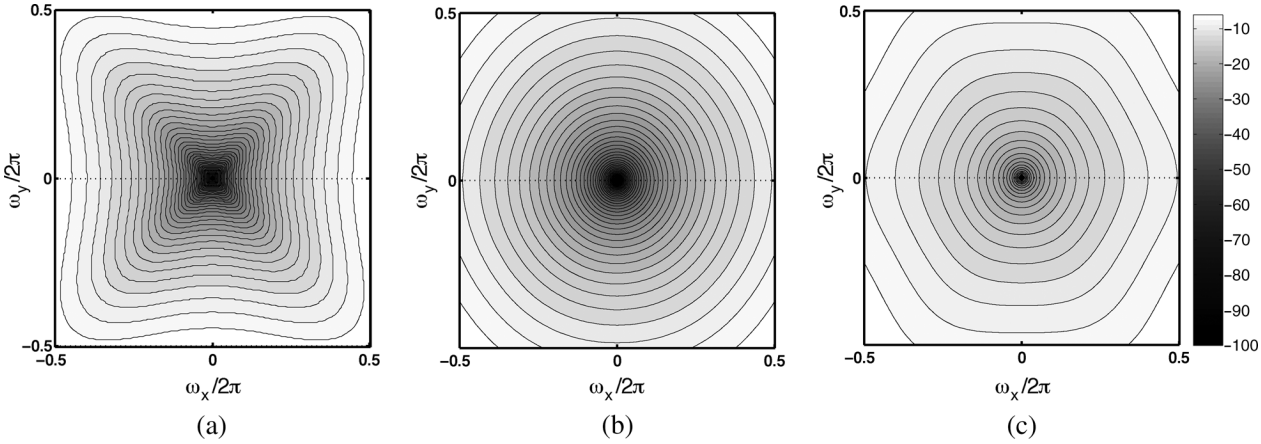

Fig. 2. Approximation error, $\kappa(\overline{\omega})$, with $-\pi/2 \leq \omega_x, \omega_y \leq \pi/2$ for (a) 2-D rectilinear, (b) triangular, and (c) hexagonal regular grids.

TABLE I
MAXIMUM AND AVERAGE APPROXIMATION ERRORS IN dB

		2D			3D			
		Rect.	Tri.	Hex.	Cubic	Tetra.	CCP	BCC
for $d=1$	$\kappa_{\max}$	-4.40	-5.51	-3.59	-4.40	-3.03	-6.01	-5.52
	κ_{avg}	-8.31	-8.41	-5.61	-8.37	-5.23	-8.56	-8.47
for $\mu=1$	$\kappa_{\max}$	-4.40	-4.95	-4.24	-4.40	-3.60	-5.10	-4.86
	κ_{avg}	-8.31	-7.84	-6.22	-8.37	-5.87	-7.63	-7.76

where $\mathbf{H}_u(\overline{\omega}) = [\mathcal{H}_{\hat{\mathbf{u}}_1}(\overline{\omega})\ \mathcal{H}_{\hat{\mathbf{u}}_2}(\overline{\omega})\ \cdots\ \mathcal{H}_{\hat{\mathbf{u}}_M}(\overline{\omega})]^{\mathbf{T}}$. Note that $\mathbf{U}^+$ is determined solely by the local topology of the mesh and is independent of spatial frequency while $\mathbf{H}$ is dependent both on the local topology and on the spatial frequency.

The approximation error is vectorial and its square magnitude can be obtained as

$$||\mathbf{E}_x(\overline{\omega})||^2 = \mathbf{E}_x^{\mathbf{H}}(\overline{\omega})\mathbf{E}_x(\overline{\omega}) \tag{17}$$

where $(\bullet)^{\mathbf{H}}$ represents the Hermitian (conjugate) transpose of the approximation error vector. This can be expressed as

$$||\mathbf{E}_x(\overline{\omega})||^2 = |F(\overline{\omega})|^2\, \mathbf{H}_u^{\mathbf{H}}(\overline{\omega})(\mathbf{U}^+)^{\mathbf{T}}\mathbf{U}^+\mathbf{H}_u(\overline{\omega}). \tag{18}$$

It is then possible to characterize the accuracy of the mesh grid by defining an error function, $\kappa(\overline{\omega})$, which is the ratio of the magnitude of the approximation error to the magnitude of the gradient of the sampled function at that spatial frequency such that

$$\kappa(\overline{\omega}) = \frac{||\mathbf{E}_x(\overline{\omega})||}{||\nabla F(\overline{\omega})||} = \frac{1}{||\overline{\omega}||}\left[\mathbf{H}_u^{\mathbf{H}}(\overline{\omega})(\mathbf{U}^+)^{\mathbf{T}}\mathbf{U}^+\mathbf{H}_u(\overline{\omega})\right]^{\frac{1}{2}}. \tag{19}$$

An average value for the approximation error function, $\overline{\kappa}(\overline{\omega})$, can be obtained by averaging $\kappa(\overline{\omega})$ for all node positions in the mesh. In a structured, regular mesh, each sample point has the same approximation error, and thus, $\overline{\kappa}(\overline{\omega}) = \kappa(\overline{\omega})$. Also, a frequency-independent error index, κ_{avg}, can be obtained by averaging the approximation error across all frequencies within the frequency bandwidth limits of the mesh grid.

III. COMPARISON OF DWM TOPOLOGIES

Although it is possible to use unstructured meshes with DWM models [6], regular meshes for which the distance between the sample points is constant are preferred as they allow simpler models with the use of unit delay elements in between junctions. There is only a limited number of regular mesh topologies in two and three dimensions.

A. The 2-D DWM Topologies

Three regular 2-D grid topologies exist: rectilinear, triangular, and hexagonal. For the triangular mesh, $M = 6$, for the rectilinear mesh, $M = 4$, and for the hexagonal mesh, $M = 3$. In all cases, $M > N$, where $N = 2$ for the 2-D setting. The reader is referred to [10] for more details of these topologies.

Fig. 2 shows the contour plot of $\kappa(\overline{\omega})$ values in logarithmic scale for the three mesh topologies. The interjunction distance $||\overline{\mathbf{r}_i}||$ for each topology is selected to be equal to a unit distance, i.e., $||\overline{\mathbf{r}_i}|| = d = 1$ to allow a comparison between topologies. If another comparison for equal mesh density (i.e., *same number of elements per unit area*) is considered, the interjunction distance for the triangular mesh will be higher than rectilinear mesh, which in turn will be higher than the hexagonal mesh. The mesh densities for the three topologies are given as $\mu_{\text{rect}} = 1/d^2$, $\mu_{\text{tri}} = 4/(3\sqrt{3}d^2)$, and $\mu_{\text{hex}} = 2/(\sqrt{3}d^2)$, for rectilinear, triangular, and hexagonal meshes, respectively [10].

The maximum and averaged error values across all spatial frequencies for different mesh topologies for the same interjunction distance, $d = 1$, and the same mesh density $\mu_{\text{rect}} = \mu_{\text{tri}} = \mu_{\text{hex}} = 1$ are summarized in Table I. When the same interjunction distance is used, the lowest approximation errors are obtained for the triangular mesh. When the mesh densities are equal, the lowest average approximation error is obtained

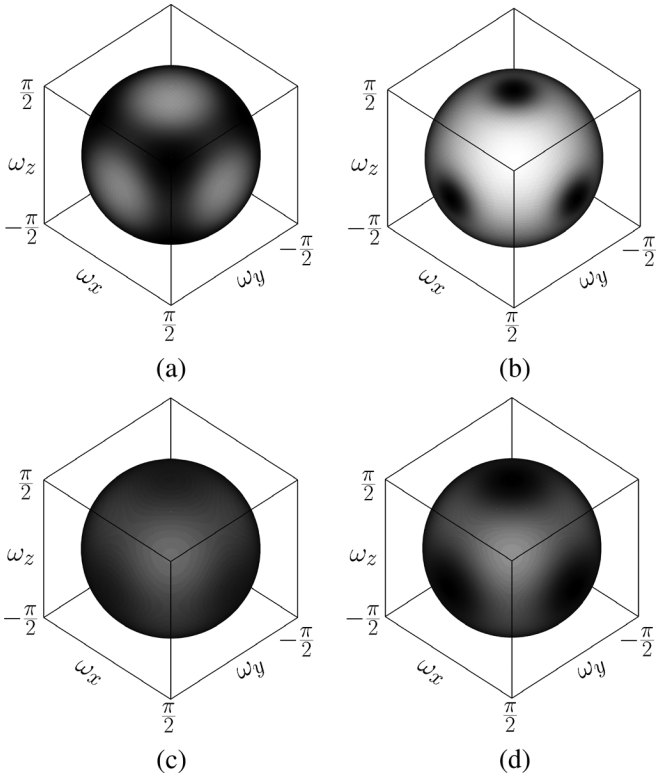

Fig. 3. Approximation error, $\kappa(\overline{\omega})$, with $-\pi/2 \leq \omega_x, \omega_y, \omega_z \leq \pi/2$ for (a) cubic, (b) tetrahedral, (c) CCP, and (d) BCC regular grids. The shading is the same for all figures, where black represents -9 dB, and white represents -3 dB.

with the rectilinear mesh, and the lowest maximum approximation error is obtained with the triangular mesh. The rectangular mesh has lower approximation errors in the diagonal directions, i.e., $\theta = (2k+1)\pi/4$. The triangular mesh has a fairly isotropic error distribution. The hexagonal mesh has lower approximation errors in $\theta = k\pi/3$ directions.

B. The 3-D DWM Topologies

There exist four regular 3-D mesh topologies: cubic, tetrahedral, body-centric cubic (BCC), and cubic close-packed (CCP). For the cubic mesh, $M = 6$, for the tetrahedral mesh, $M = 4$, for the BCC mesh, $M = 8$, and for the CCP mesh, $M = 12$. As with the 2-D case, $M > N$ for all topologies with $N = 3$. The reader is referred to [9] for the details of these topologies.

Fig. 3 shows the visualization of $\kappa(\overline{\omega})$ values in logarithmic scale for the four 3-D mesh topologies at $||\overline{\omega}|| = \pi/2$. The interjunction distance $||\overline{\mathbf{r}_i}||$ for each topology is selected to be equal to a unit distance, i.e., $||\overline{\mathbf{r}_i}|| = d = 1$, to allow a comparison between topologies. Another comparison is also made for the same mesh density in all topologies. Mesh densities for the 3-D topologies are given as $\mu_{\text{cubic}} = 1/d^3$, $\mu_{\text{tetra}} = 3\sqrt{3}/(8d^3)$, $\mu_{\text{BCC}} = \sqrt{2}/d^3$, and $\mu_{\text{CCP}} = 3\sqrt{3}/(4d^3)$, for cubic, tetrahedral, CCP, and BCC topologies, respectively [9].

The maximum and averaged approximation error values across all spatial frequencies for different mesh topologies for the same interjunction distance and same mesh density (i.e., *same number of elements per unit volume*) $\mu_{\text{cubic}} = \mu_{\text{tetra}} = \mu_{\text{BCC}} = \mu_{\text{CCP}} = 1$ are summarized in Table I. It may be observed that the lowest errors are obtained for the CCP topology when the same interjunction spacing is used. On the other hand, while the mesh densities are the same, the average error is the lowest for the cubic mesh and the maximum error is lowest for the CCP mesh.

IV. Conclusions

A comparison of different multidimensional digital waveguide mesh topologies with respect to the accuracy of numerical derivatives was presented in this letter. The derivation of the numerical derivatives in a general N-dimensional mesh was given. A measure for quantifying the approximation error in the spatial frequency domain was proposed. The results were applied to regular DWM grid topologies in 2-D and 3-D. In 2-D, the rectilinear, triangular, and hexagonal mesh topologies were compared. In 3-D, cubic, tetrahedral, CCP, and BCC, mesh topologies were compared. The results suggest that for the same internodal distance, the triangular mesh in 2-D and the CCP mesh in 3-D have lower approximation errors. For the same mesh density, rectilinear mesh in 2-D and cubic mesh in 3-D have the lowest average errors. However, the triangular mesh in 2-D and CCP mesh in 3-D have the lowest maximum approximation error. Although the comparison was given for the regular mesh structures only, the results are general and are readily applicable to unstructured mesh topologies.

Acknowledgment

The authors would like to thank Prof. V. Välimäki and three anonymous reviewers for their feedback and constructive comments.

References

[1] J. Mullen, D. M. Howard, and D. T. Murphy, "Real-time dynamic articulations in the 2-D waveguide mesh vocal tract model," *IEEE Trans. Audio, Speech, Lang. Process.*, vol. 15, no. 2, pp. 577–585, Feb. 2007.

[2] C. Erkut, "Aspects in analysis and model-based sound synthesis of plucked string instruments," Ph.D. dissertation, Helsinki Univ. Technol., Helsinki, Finland, Nov. 2002.

[3] F. Fontana and D. Rocchesso, "Physical modeling of membranes for percussion instruments," *Acta Acustica united with Acustica*, vol. 83, no. 3, pp. 529–542, May-Jun. 1998.

[4] L. Savioja and V. Välimäki, "Interpolated rectangular 3-D digital waveguide mesh algorithms with frequency warping," *IEEE Trans. Speech Audio Process.*, vol. 11, no. 6, pp. 783–790, Nov. 2003.

[5] H. Hacıhabiboğlu, B. Günel, and A. M. Kondoz, "Source directivity simulation in digital waveguide mesh-based room acoustics models," in *Proc. AES 30th Int. Conf. Intelligent Audio Environments*, Mar. 15–17, 2007, on CD-ROM.

[6] S. Bilbao, *Wave and Scattering Methods for Numerical Simulation*. Chichester, U.K.: Wiley, 2004.

[7] A. D. Pierce, *Acoustics: An Introduction to Its Physical Principles and Applications*. Woodbury, NY: Acoust. Soc. Amer., 1994.

[8] R. H. MacNeal, "An asymmetrical finite difference network," *Quart. Appl. Math.*, vol. 11, no. 3, pp. 295–310, 1953.

[9] G. R. Campos and D. M. Howard, "On the computational efficiency of different waveguide mesh topologies for room acoustics simulation," *IEEE Trans. Speech Audio Process.*, vol. 13, no. 5, pp. 1063–1072, Sep. 2005.

[10] F. Fontana and D. Rocchesso, "Signal-theoretic characterization of waveguide mesh geometries for models of two-dimensional wave propagation in elastic media," *IEEE Trans. Speech Audio Process.*, vol. 9, no. 2, pp. 152–161, Feb. 2001.